Atmospheric Research 266 (2022) 105968

Contents lists available at ScienceDirect

Atmospheric Research

journal homepage: www.elsevier.com/locate/atmosres

Spatial variation of catchment-oriented extreme rainfall in England and Wales

H. Wang [a], Y. Xuan [a,*]

[a] Zienkiewicz Centre for Computational Engineering, Swansea University Bay Campus, Fabian Way, Swansea SA1 8EN, UK

ARTICLE INFO

Keywords:
Spatial variation
Century-long variation
Catchment-orientated annual maximum daily rainfall
GEV

ABSTRACT

This paper presents the spatial variation of the annual maximum daily rainfall (AMDR) in more than 900 catchments of England and Wales over the last century with respect to different spatial features including geographic location, elevation, size, orientation and shape of catchments. A spatial pattern extraction and recognition (SPER) toolbox is employed to extract the spatial features of catchments where the AMDR is modelled by a well-tested Generalized Extreme Value (GEV) distribution. The results show that the GEV parameters μ and σ exhibit similar patterns and are usually larger with higher elevations. Increasing catchment size can decrease parameters due to areal averaging, however, in the middle-sized transition regions of the rainfall variation, e.g., east Wales, the trend reverses. For areas at higher elevation, parameters are greater in the west-northwest-oriented catchments while parameters in west-northwest or east-northeast-oriented catchments at lower elevation are similar or smaller than those with a north-south orientation. An elongated shape catchment usually has smaller parameters than a rounded-shape one. These findings reveal the heterogeneity of extreme rainfall distribution in space with respect to different spatial characteristics of catchments even under the same climate, which lays a basis for further catchment-based analysis concerning the relationship between hydrological response and geomorphic properties.

1. Introduction

Extreme rainfall events have been observed to become more frequent since the 1950s in many regions of the world, which is challenging the current storm design practices (Burn et al., 2011; Stott et al., 2016; Taylor et al., 2017). Quantifying the behaviour of flood-triggering rainfall at extreme levels is an essential step in flood risk management (FRM; Coles and Tawn, 1996). Although rainfall as one part of the global hydrological circle that is boundless, FRM is usually carried out at different scales associated with one or several regions of interest which are defined within a hydrological or political boundary (Elsebaie, 2012). Therefore, the analysis on rainfall variation studied at various scales such as city, country, climatic zone and the globe is very important and of concern of flood risk managers and stakeholders (Kumar et al., 2010; Phuong et al., 2019). In recent decades, many studies focused on the variability of rainfall in time and space at different scales based on gauged records (Buishand et al., 2008; Jung et al., 2017; Pedersen et al., 2010; Villarini et al., 2010; Zheng et al., 2016). For example, Archer and Fowler (2018) broke the long-term gauged rainfall and streamflow datasets of Great Britain into two scenarios and selected five events to illustrate typical characteristics of rainfall-runoff regarding different geographic locations; other researchers analyzed gauged rainfall extremes corresponding to their hydrological response in the river catchments of different sizes (Anquetin et al., 2010; Lobligeois et al., 2014; Sangati et al., 2009).

Thanks to the advances in environmental monitoring technology, more spatially disaggregated, grid-based hydro-climatic datasets have become more accessible to the research community with steady improvements in both spatial-temporal resolution and quality, including those from weather radars such as the NIMROD system (Fairman Jr et al., 2017), satellite, such as GPM (Islam et al., 2014), as well as those from model simulations. Therefore, processing these huge-sized data to support large scale variation analysis of grid-by-grid hydroclimatic extremes which contains high risks has become an important issue to address (Peleg et al., 2018). One of such examples is the series of publications from the UK Climate Impacts Programme (UKCIP) (Banwell et al., 2018; Kendon et al., 2019; Lowe et al., 2018) where analyses over climate model (CM) grids are aggregated over various political regions

* Corresponding author.
E-mail address: y.xuan@swansea.ac.uk (Y. Xuan).

https://doi.org/10.1016/j.atmosres.2021.105968
Received 20 August 2021; Received in revised form 19 November 2021; Accepted 7 December 2021
Available online 11 December 2021

to provide support to stakeholders and local governments. Prein et al. (2017) studied the observed and simulated changes in local precipitation extremes over the contiguous US. Wang and Xuan (2020) randomly generated a large number of regions of interest and quantified the grid-based rainfall extremes with respect to regions' location, size and shape over the last century in Great Britain and Australia. Therefore it is clear that the variation of the spatial distribution of area-oriented rainfall is not only closely related to the climate (Batisani and Yarnal, 2010), its local features and processes such as the topography, urbanization and the scale and orientation of the study regions can also affect the rainfall amount (Buytaert et al., 2006; Tomasella et al., 2019).

Although there is an increasing number of applications in these new available, large-scaled, grid-based data, these efforts are often frustrated by the insufficient length of the required data records and most studies focus only on the spatiotemporal quantification of rainfall at the average level instead of the extremes. For the extreme rainfall studies, most of them suffer from a limited number of study regions therefore the exploration and comparison of different locative features that can affect rainfall extremes are not generalized. For example, many studies have analyzed and indicated the links between the extreme rainfall and spatial factors such as slopes and elevation (Johansson and Chen, 2003; Sanchez-Moreno et al., 2014; Staub et al., 2014), however, additional factors such as the direction of rainfall storms, the shape and orientation of catchments that are also recognized as significant factors in runoff generation (Shaw, 2005), have yet been fully studied especially at the extreme level. Besides, testing and quantifying the long-term changes at such level by using grid-based data is a significant and not-fully studied topic as well.

Motivated by these, we made use of a century-long grid-based rainfall dataset with high spatial and temporal resolutions (1×1 km^2 and daily), and more than 900 catchments in Great Britain (GB), aiming to quantify the behaviour of catchment-based rainfall extremes in the last century. To the concern of great importance in the engineering design, we address how rainfall extremes are affected by the catchment features i.e., geographic location, elevation, size, shape and orientation. A toolbox known as the Spatial Pattern Extraction and Recognition (SPER) developed by the authors is employed for extracting the spatial features of these catchments. Then the annual maximum daily rainfall (AMDR) of each catchment is extracted and fitted with the widely used and tested Generalized Extreme Value (GEV) distributions of which the spatial variation is then analyzed with regards to the GEV parameters. This procedure is assisted with the high-performance computing (HPC) resources provided by Super Computing Wales (https://www.supercomputing.wales) due to the huge size of the datasets and the intensive computation demand.

The remainder of this paper is organized as follows: Section 2 describes the data and methods. Then the spatial features of catchments and the simulation results of the AMDR fitted by the GEV model are analyzed in section 3.1. Both the qualitative and quantitative results of spatial variation of AMDR with respect to catchment location, size, shape and orientation, represented by the parameters are presented in detail in section 3. Finally, the results are further discussed in section 4 while the conclusions and recommendations of future study and applications are given in section 5.

2. Materials and methods

2.1. Datasets and catchments

This study makes use of two datasets: one is the century-long dataset named the "Gridded Estimates of daily Areal Rainfall" (GEAR) which is derived from the UK Met Office national database of observed precipitation from the UK rain gauge network using the natural neighbour interpolation method; and the other is the grid-based elevation data named as "Ordnance Survey Terrain 5" (OS Terrain 5) covering the whole Great Britain (GB).

The GEAR dataset is a grid-based (1×1km^2) rainfall estimation covering the mainland of GB from 01/01/1898 to 31/12/2010 and the coordinates are the National Grid Reference (Survey, 1946) which is a projected map coordinate system with the easting (x-) and northing (y-) expressed in linear kilometres (Tanguy et al., 2016). The geographical origin of the GEAR data matrix starts from the location of 400 km west, 100 km north of the true Origin (49°N, 2°W), spreading 700 km eastward and 1250 km northward. The recorded rainfall values are provided as daily rainfall, i.e. the total rainfall amount over a predefined 24-h (9 AM–9 AM) period which refers to the 24 h after the reporting day.

The OS Terrain 5 dataset is supplied as a whole set of GB divided into 5 km by 5 km tiles. These tiles are identified by quoting the National Grid reference of the southwest corner of the area they cover and the dataset is published as both grid (with 5-m post spacing) and contours (with 5-m interval). In this study, we apply the grid type where each tile includes 100 by 100 (10000) grids whose size is 50×50 m^2. In this study, to make the spatial resolution of two datasets consistent, we convert the resolution of the OS Terrain 5 data by firstly resampling the OS Terrain 5 data in the 50×50 m^2 grids, and then taking the average of height to match the 1×1km^2 grids of the GEAR dataset. The comparison of conversion is presented in the supplementary Fig. S1.

In this study, the shapefiles for recording the boundary of the 903 catchments of England and Wales are provided by the UK Centre for Ecology and Hydrology (Morris and Flavin, 1990) in the same coordinates (i.e., the National Grid Reference) with the GEAR data and shown in Fig. 1.

2.2. Method

Fig. 2 presents the four steps of this study which are specified as:

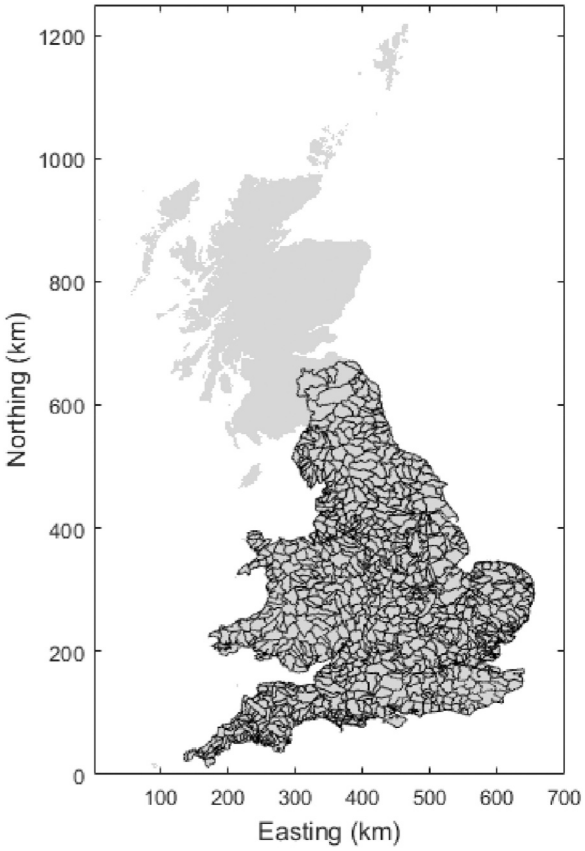

Fig. 1. The 903 catchments in England and Wales.

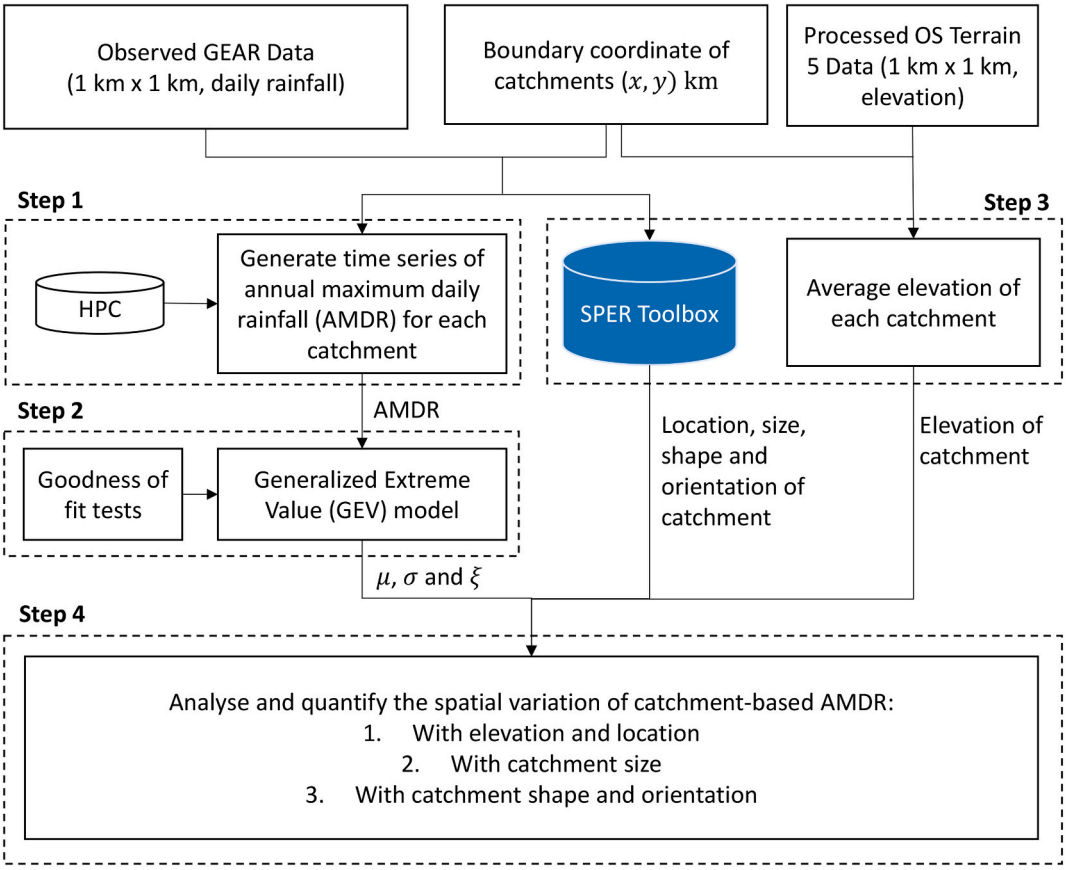

Fig. 2. The four-step methodology of the study.

1) Extract the time series of annual maximum daily rainfall (AMDR) of each catchment with the assistance of high-performance computing (HPC).
2) Fit the time series obtained at every catchment with generalized extreme value distribution with the goodness of fit tested by bootstrapping KS and AD tests.
3) Extract the spatial features (location, size, shape and orientation of catchment) by employing the SPER toolbox and elevation by using OS Terrain 5 Data directly.
4) Analyse how the spatial features affect the spatial dependency of areal rainfall extremes.

2.2.1. Time series extraction and HPC involvement

For each catchment, the areal daily rainfall is calculated by taking the arithmetic average. The maximum value of each year is then selected to generate the annual maxima series, i.e., annual maximum daily rainfall, (AMDR). There is a huge amount of data to be processed, e.g., around 600 gigabytes of grid-based daily rainfall data (1 × 1 km, 365 days/year, 113 years) covering the UK and 903 catchments in our case, which causes a heavy overhead of a typical desktop PC that usually features 4 processing cores and a limited memory capacity. To increase the operation efficiency, we employed supercomputers from the High-performance Computing (HPC) Wales (https://www.supercomputing.wales) to assist the extraction of the data. The supercomputing hubs of HPC Wales have a total of 13,080 processing cores, connecting to high-speed memory and storage, and can deliver 1 petaflop of computing power (Flanagan et al., 2020). Supercomputers of HPC Wales are Linux-powered and use the Slurm batch scheduler/script to allocate and push the jobs or programme to supercomputers and run (more operation details can be checked in https://portal.supercomputing.wales/). In this study, the programme for extracting catchment rainfall is coded in Python and multiprocess is used for paralleling the jobs to increase the computation speed.

2.2.2. Generalized Extreme Value (GEV) model and goodness of fit tests

The AMDR time series extracted at each catchment is fitted by the GEV distribution whose cumulative distribution function (CDF) is defined as (Embrechts et al., 2013):

$$F(x;\sigma,\mu,\xi) = \begin{cases} exp\left[-\left(1+\xi\left(\frac{x-\mu}{\sigma}\right)\right)^{-\frac{1}{\xi}}\right] \text{ for } \xi \neq 0 \\ exp\left[-exp\left(-\frac{x-\mu}{\sigma}\right)\right] \text{ for } \xi = 0 \end{cases}, \quad (1)$$

F is defined for $1+\xi(x-\mu)/\sigma > 0$, $-\infty < \mu < \infty$, $\sigma > 0$ and $-\infty < \xi < \infty$, where μ is the location parameter, σ is the scale parameter, and ξ is the shape parameter (De Haan et al., 2006). There are three types of distribution in the GEV family, which are distinguished by their shape parameters (Coles et al., 2001). The type I distribution, also known as the Gumbel distribution, refers to the case where $\xi = 0$; while the types II and III are known as the Fréchet distribution and the Weibull distribution corresponding to the cases where $\xi > 0$ and $\xi < 0$ respectively. These three parameters are estimated by using Maximum likelihood method.

It is worth revisiting the implication of parameters of the GEV models. The location parameter μ indicates the mode of the time series which is consistent with the most frequent AMDR in our cases, while the scale parameter σ indicates its average dispersion for each AMDR from μ (equals $\sqrt{6}/\pi$ multiplying by the standard deviation if $\xi = 0$) (Izaguirre et al., 2010). In other words, the larger σ, the more spread-out the distribution is. Conversely, the smaller the parameter, the more compressed the distribution is (Kantar and Şenoğlu, 2008; Mann, 1967). In our study, if σ is estimated to be increasing, the occurrence probability of

extreme AMDR, i.e. rainfall ranked in the higher positions will also increase.

To test whether GEV can fit the time series of AMDR well, we employed two different methods: the Kolmogorov-Smirnov (KS) test (Kolmogorov, 1933; Smirnov, 1948) and Anderson-Darling (AD) test (Anderson and Darling, 1952, 1954). These two tests have been widely used to test whether a given data sample is drawn from a particular type of probability distribution (the reference distribution). In this case, the reference distribution is GEV distribution and the null hypothesis H_0 for both tests is that the AMDR X $(x_1, x_2, \ldots, x_n)$ is drawn from GEV distribution and the alternative hypothesis H_1 states against H_0. Besides, the L-moment ratio diagrams are also employed to compare the fitted GEV distribution with the statistical characteristics of AMDR itself.

2.2.2.1. KS test. The KS test detects the greatest vertical distance, the so-called KS test statistic (D_n), between empirical cumulative distribution function of the observed AMDR $F_n(x)$ and the cumulative distribution function of the reference GEV distribution $F(x)$. The equation for test statistics is given by (Kolmogorov, 1933; Smirnov, 1948):

$$D_n = \sup_x |F_n(x) - F(x)| \tag{2}$$

where $\sup_x$ is the least upper bound of the set of distances. $F_n(x)$ can be calculated by $\frac{1}{n}\sum_{i=1}^{n} I_{X_i \le x}$ where $I_{X_i \le x}$ is an indicator function and equals 1 if $X_i \le x$ or 0 if otherwise. If H_0 holds, D_n tend to be small. Conversely, large values of D_n are expected. The criteria are to reject the null hypothesis at a 0.05 significance level if D_n is greater than the critical value (0.198).

2.2.2.2. AD test. Similar to the KS test, the AD statistic (A^2) is used in the AD test to detect how well the data follow a reference distribution, i.e., GEV distribution in this study. The smaller A^2 indicates a better fitness of the data by given distribution. Different from the KS test, the AD test weights more heavily in the tails of the distribution for extreme data and A^2 is given as (Anderson and Darling, 1954):

$$A^2 = -n - \frac{1}{n}\sum_{i=1}^{n}(2i-1)\{lnF(X_i) + ln[1 - F(X_{n-i+1})]\}, \tag{3}$$

If A^2 is greater than the critical value (2.502) at the 0.05 significance level, the null hypothesis is rejected. The critical value is approximated depending on the sample size only and not on the distribution.

2.2.3. Bootstrapping technique involved in the goodness of fit tests

One of the most significant limitations when using the non-parametric KS test in evaluating the fitness is that the reference distribution (i.e., the reference GEV distribution $F(x)$ in Eq. 2) has to be fully specified and data-independent (Fasano and Franceschini, 1987). In other words, the KS test becomes invalid if the three GEV parameters are estimated using the same data whose distribution is going to be tested. Therefore, the challenge is how to determine the reference GEV distribution appropriately. One possible approach is to use the bootstrapping technique to simulate the reference. We broadly followed Lilliefors (1967) and developed a bootstrapping method to establish the reference distribution under the null hypothesis H_0 and the general procedure can be found in Eduardo (2020).

Step 1: Estimate a set of parameters $\widehat{\theta}$ of the GEV distribution, from the sample of AMDR (x_1, x_2, …, x_n) by using the maximum likelihood (ML) method;

Step 2: Compute the KS statistic D_n from $\boldsymbol{X}$ and the cumulative distribution function (CDF) of the GEV distribution with the parameters of $\widehat{\theta}$, e.g., $F_{\widehat{\theta}}$;

Step 3: Perform bootstrap resampling for a predefined number of times J; for each iteration $j = 1, 2, \ldots, 5000$:

1. simulate a bootstrapped sample (x_{1j}, x_{2j}, …, x_{nj}) from $F_{\widehat{\theta}}$;
2. estimate a new set of parameters $\widehat{\theta}_j$ from the bootstrapped sample (x_{1j}, x_{2j}, …, x_{nj}) using the same ML method;
3. compute the statistic D_{nj} from (x_{1j}, x_{2j}, …, x_{nj}) and $F_{\widehat{\theta}_j}$;

Step 4: Obtain the p-value approximation:

$$p - \text{value} \approx \frac{1}{J}\sum_{j=1}^{J} 1_{D_{nj} > D_n}, \tag{4}$$

2.2.4. Spatial feature extraction using the SPER toolbox

The spatial pattern extraction and recognition (SPER) toolbox is an effective tool developed to provide an automatic extraction and classification of hydroclimatic patterns by their spatial features i.e., location, size, orientation, and shape, as well as the physical features, i.e., the areal average, total volume, the spatial distribution. We employed the stable algorithm incorporated in the toolbox for automatically identifying the spatial features of catchments that are linked to rainfall extremes. Since the boundary has already been predefined by the catchment shapefiles (see Fig. 3) which are the inputs of the toolbox, the rainfall grids inside this boundary are then regarded as the region of interest (ROI) where areal AMDR is extracted with the assistance of HPC. In the meantime, a four-step algorithm is carried out, corresponding to four outputs and more details can be seen in supplementary Text S1. The location of the catchment is represented by the coordinates of its geometric centroids consistent with the GEAR dataset and the size is calculated as the product of the number of inside grids and the grid size (i.e., the resolution). The toolbox can also find the two principal axes of an ROI along which the product of inertia of ROI is zero and the longer axis is the major one while the shorter is the minor perpendicular to the major axis. The orientation of ROI (see ω in Fig. 3) is then defined as the angle of the major axis from the North in a clockwise direction (i.e., northeast, positive) and anti-clockwise direction (i.e., northwest, negative). Finally, the minimum encompassing rectangle is identified by the toolbox (see the green rectangle in Fig. 3) and the shape of ROI (sp) is indexed by the ratio of the height divided by the width, which is used to characterise the elongation of the ROI.

An example catchment is demonstrated in Fig. 3. For each catchment there are three indexes for representing the three spatial features: 1) location index (x- and y- of the geometric centroid, e.g., Easting 301.59 km, Northing 318.56 km); 2) size index s (e.g., 190 km^2); 3) orientation index ω (Northwest 51.05°) and shape index sp (e.g., 2.59 which is regarded as a relatively elongated shape).

3. Results and discussions

3.1. Spatial features of catchments in England and Wales

The suitability of GEV is assessed by using the bootstrapping KS and AD tests. The distribution of the p-value of all catchments is calculated by both tests as shown in Fig. 4a where the p-value indicates the percentage of iteration when the null hypothesis cannot be rejected at the significant level of 0.05. The results show that the GEV distribution can fit well as the p-value in the majority of cases is closed to 1 and more than 95% of cases pass the KS and AD tests.

The subfigures b, c, d and e of Fig. 4 present the spatial distribution of catchments with respect to their spatial features, i.e., the elevation H, size S, orientation angle ω and shape sp. The highest elevation is observed in the Scottish Highland, generally more than 800 m. Then North England and North Wales are also relatively high with an average elevation higher than 400 m and the rest of England is the lowest. In addition, it can be observed that the size of most catchments (around 99%) in England and Wales are less than 600 km^2 while only the catchments located near the boundary between England and Scotland have a larger size which is greater than 1000 km^2. The catchment sizes

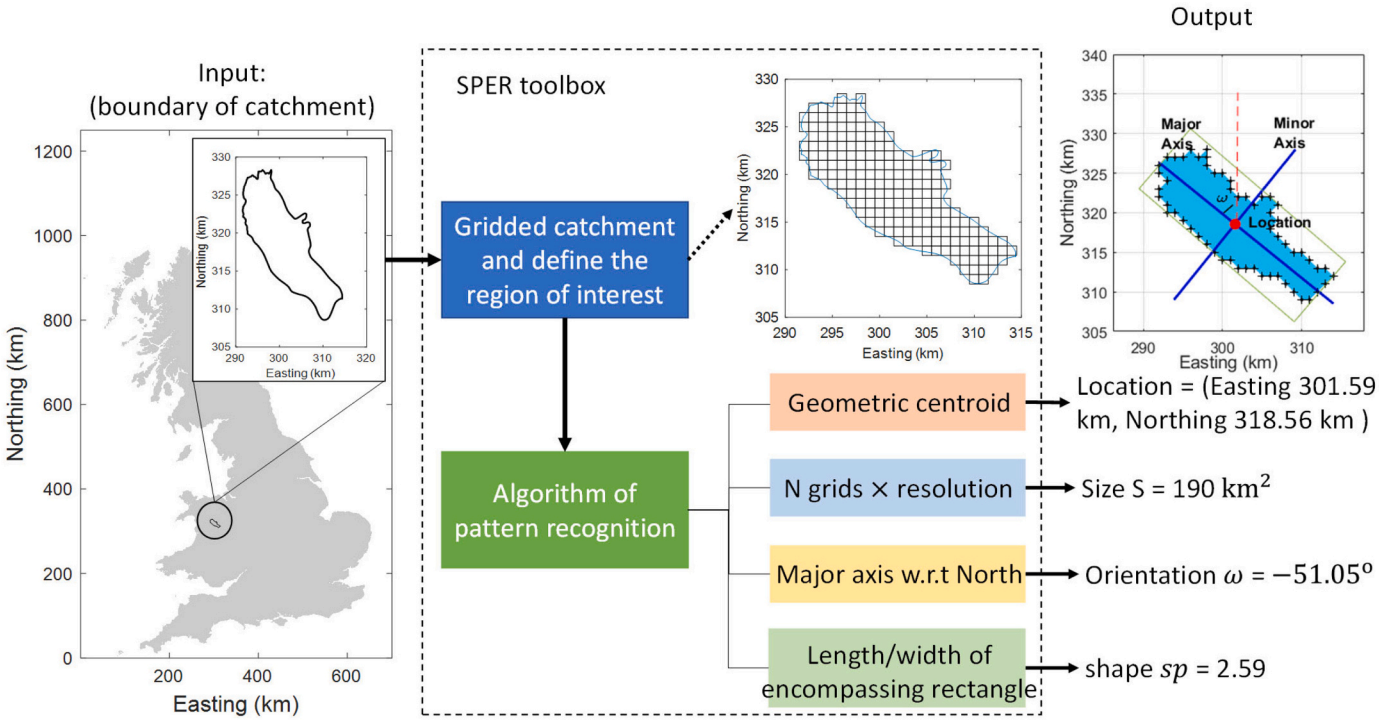

Fig. 3. The SPER toolbox and its application on the catchment-based analysis.

vary greatly because these catchments are actually sub-catchments of the same river basin. The orientation of these catchments is indicated by the major angle ω referring to the North direction. In other words, $\omega = 0$ indicates the orientation of catchment is north-south direction; the positive ω (presented by reddish colour) indicates a north-east orientation while the negative angle (presented by bluish colour) is a north-west orientation; and ω equaling to $\pm 90^{o}$ means the orientation of catchment is east-west direction. It can be observed that the catchments near the north coastlines tend to be northeast orientated while the ones near east coastlines are northwest orientated. Moreover, the catchments located at the boundary of Wales and England tend to be north-south orientated indicating a very light red or blue colour (i.e., ω closed to 0). Referring to the shape of catchments shown in Fig. 4d, the shape of most catchments (61%) is relative rounded or elliptical and their *sp* is in the range of 1.0 and 2.0. *sp* to the rest majority is less than 4.0 indicating an elongated shape.

To explore more about the catchment characteristics, Fig. 4f and Fig. 4g are generated where the spread of the shape index *sp* of smaller regions is greater than that of larger regions; while the elongated shape has a much higher probability of being accompanied with a small size, the large size of catchment tends to have a relatively rounded shape in both England and Wales. The relationship between the catchment shape and orientation is insignificant although the catchments with an elongated shape tend to have a northwest or northeast orientation (ω around $\pm 50^{o}$).

3.2. Spatial variation of AMDR with respect to location and elevation

Fig. 5 presents the spatial patterns of the AMDR represented by the three GEV parameters in the catchments over England and Wales (a, b and c); and how these parameters are related to the catchment elevation (d, e and f). Out of all catchments, there are around 80% follow the Fréchet distribution ($\xi > 0$, shown in reddish colour in Fig. 3a), mainly located in middle and eastern England of lower elevation; only 16% follow the reversed Weibull distribution ($\xi < 0$, shown in bluish colour), mainly located in the vicinity of Manchester and Liverpool and middle-western Wales where the elevation is relatively high (see Fig. 4b); and the rest (4%) following Gumbel distribution ($\xi = 0$).

Subfigures b and c of Fig. 5 present the spatial variation of the GEV parameters σ and μ by which the behaviour of AMDR can be parameterised and depicted. It can be observed that both σ and μ present a similar spatial pattern where a higher μ is usually accompanied by a higher σ. Meanwhile, along the same Northing coordinate, the parameters of the western region, especially in western Wales and the Lake District of England, are much greater than those of the eastern area such as middle and east England. By contrast, the change of the parameters in the catchments located at the same Easting coordinate is not remarkable and the only difference is that σ and μ of the catchments in North England are higher than the South areas. Such spatial pattern can be described as "west high, east low" and the difference is not linearly either - there is a significant decrease occurring in the west while the gradient of such decrease is much smaller in the east. As μ can reflect the level of the most frequent AMDR in the last century and σ can somehow tell the occurrence probability of those extreme events, the parameterization quantification can be translated as: the most frequent AMDR in the west is usually higher than the east and those areas with a higher most frequent AMDR are usually observed to have a higher probability of the occurrence of extreme AMDR. The corresponding Fig. 5e and 5f are presented to show the general relationship between the GEV parameters and the catchment elevation *H* which is demonstrated by trend lines. In general, both parameters have a positive trend that catchments with a higher elevation have a higher level of most frequent AMDR as well as a higher occurrence probability of extremes. A plausible explanation is that the local topography can play an important role in enhancing extreme rainfall via processes such as the uplifting of moist air.

3.3. Spatial variation of AMDR with respect to catchment size

The UK Meteorological Office usually classifies rainfall into four categories according to the rate of precipitation (Jebson, 2007): "slight" (0~2 mm/h or roughly 0~5 mm/day), "moderate" (2~10 mm/h or 5~25 mm/day), "heavy" (10~50 mm/h or 25~125 mm/day), and "violent" (>50 mm/h or 125 mm/day). To be more specific, in this

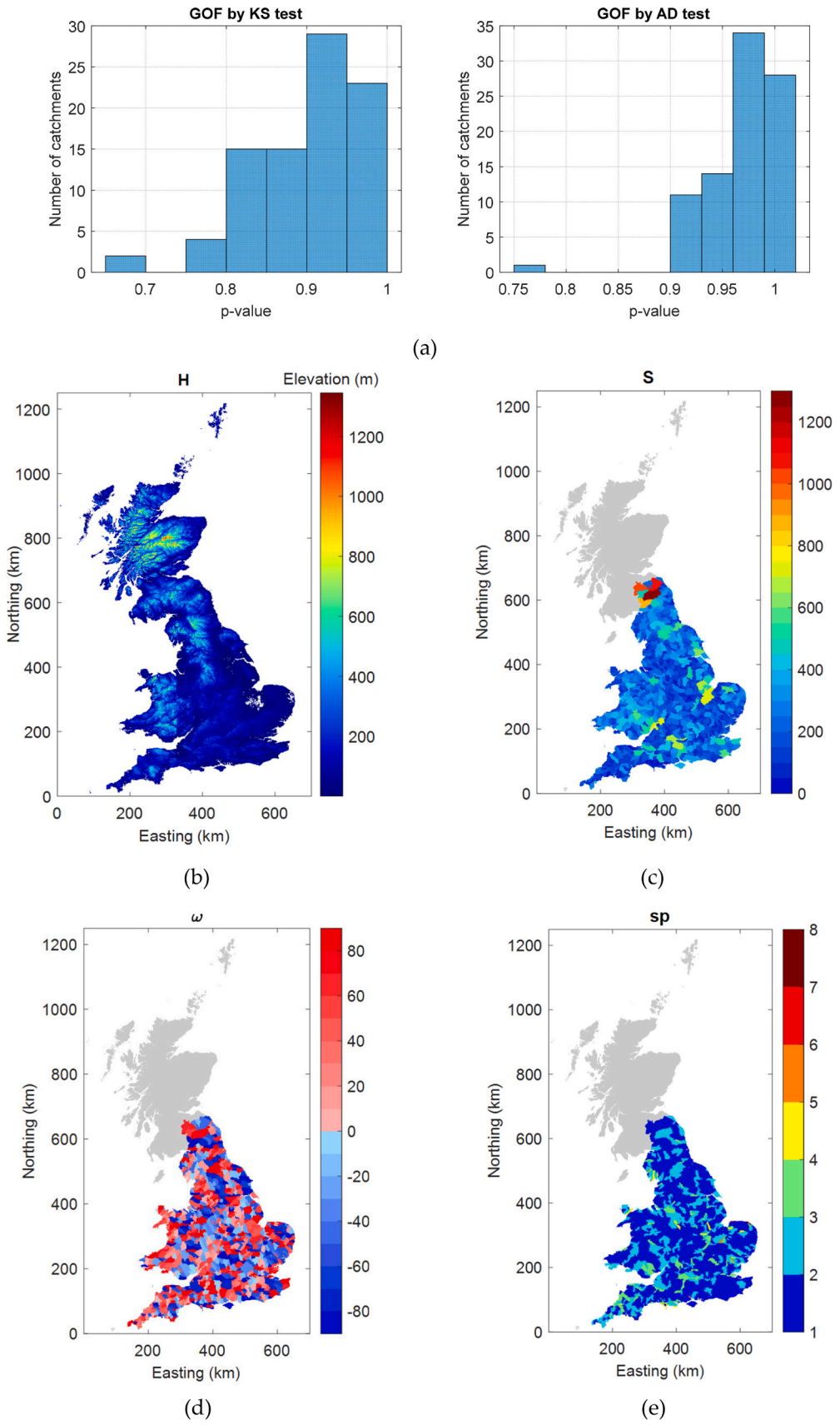

Fig. 4. The goodness of fit test results (a) and spatial features of study catchments (b-g).

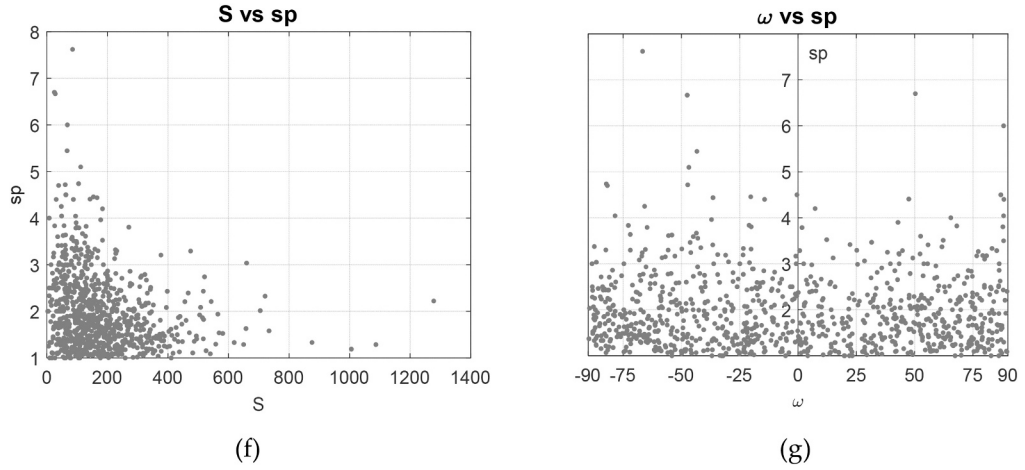

Fig. 4. (*continued*).

study, we added several classes and divided the catchment-based AMDR at the most frequent level (w.r.t. μ) into 5 groups, i.e., slight (<10 mm/day, 1.0% of all catchments), moderate (10~25 mm/day, 25.6%), high (25~50 mm/day, 70.3%), extreme (50~100 mm/day, 3.0%), very extreme (>100 mm/day, 0.1%). The location of catchments belonging to these five groups as well as the GEV parameters σ and μ changing over catchment size are shown in Fig. 6, respectively. Catchments with moderate AMDR level are mainly located in east England while those at the extreme level are located in the Lake District and North and West Wales near the coast.

In general, with the increase of catchment size, both parameters show a decreasing trend especially in the south and east England ("Moderate" group), middle-west Wales and the Lake District ("Extreme" group), which is caused by areal averaging and the same with the ROI-based study. However, for the "High" group with a middle level of the most frequent AMDR, a decreasing trend can be observed when the catchment size is either relatively small (e.g., less than 200 km^2) or relatively large (e.g., greater than 500 km^2). However, there is an increasing trend shown in the catchments of medium sizes (400– 500 km^2). This phenomenon shows that the change of parameters over catchment sizes is strongly affected by their geographic locations. For example, for the catchments in this group (those mainly located near the boundary of the high and extreme AMDR areas; see the catchments with the size of 400– 500 km^2 in Wales and southern England in Fig. 4c), if increasing the catchment size involves more grids with higher AMDR, the corresponding parameters μ and σ will also increase because the reduction caused by areal averaging cannot be compensated by the involvement of more heterogeneous grids of higher rainfall. Such effect can go the other way as well when more grids of lower AMDR are included. This can explain the result for the "Extreme" group where an increasing trend is observed when the size is in the range of 200– 300 km^2. For the small catchments located in the Lake District and middle-west Wales where the AMDR are extreme, larger catchments tend to include more grids with higher rainfall thereby increasing μ and σ.

3.4. Spatial variation of AMDR with respect to catchment orientation and shape

Comparing with the location, elevation and size of the catchments, the effect of catchment orientation and shape is not that significant; however, in order to demonstrate such relation more clearly, we fit the result using local linear regression (LLR; Baíllo and Grané, 2009; Fan, 1993) as the background of subfigures in Fig. 7 to help the analysis. One of the most commonly used methods for carrying out LLR is Locally Weighted Scatterplot Smoothing (LOWESS; Cleveland, 1979; Moran, 1984) which can generate a smooth curve or surface to help figure out the relationship or trend between the two GEV parameters and the catchment features, i.e., the orientation and shape in this case. More details of the procedure and residual analysis are included in supplementary Text S2.

For the catchments in the "Moderate" group, there is a small difference between the west-northwest oriented and east-northeast oriented catchments on σ and μ which tend to be smaller than that of the north orientation. However, both σ and μ tend to decrease when the shape becomes more and more elongated. For those in the "High" group, the majority of the catchments show small differences on both parameters between the west-northwest and east-northeast orientation while the μ parameters for the catchments with north-northeast orientation are usually higher than those of the catchments with north-northwest orientation. Generally, the two parameters decrease with an increased *sp* but smaller-sized catchments witness a converse trend. For the "Extreme" group, the pattern of the parameters changing over the orientation is distributed symmetrically with $\omega = 0$ (North) where catchments with a west-northwest orientation usually have higher parameters than east-northeast orientation. On the whole, several patterns can be summarised as:

1) In middle-west Wales and the Lake District of England where AMDR is high, both levels of the most frequent AMDR and occurrence probability of extremes are higher in the catchment orientated in a west-northwest direction than others.
2) For the rest area of Wales and England, generally, the level of the most frequent AMDR and occurrence probability of extremes in the catchments whose orientations are west-northwest or east-northeast are almost the same and lower than that the north-south oriented catchments.
3) The level of the most frequent AMDR and occurrence probability of extremes in the catchments with an elongated shape are usually lower than others with a relatively rounded shape.
4) Catchment orientation and shape are not as much significant as their locations and sizes concerning the spatial effect on AMDR.

4. Discussion

In recent decades, many efforts have been devoted to improving the performance of physically-based models such as the rainfall-runoff model in simulating and forecasting floods by optimizing the complexity of the structure, refining the spatial and temporal resolution, even involving various data-driven techniques e.g., machine learning. They aim to gain a better understanding and description of the real world. However, the simulation path of physical-based models can inevitably associate with uncertainties that can propagate and lead to

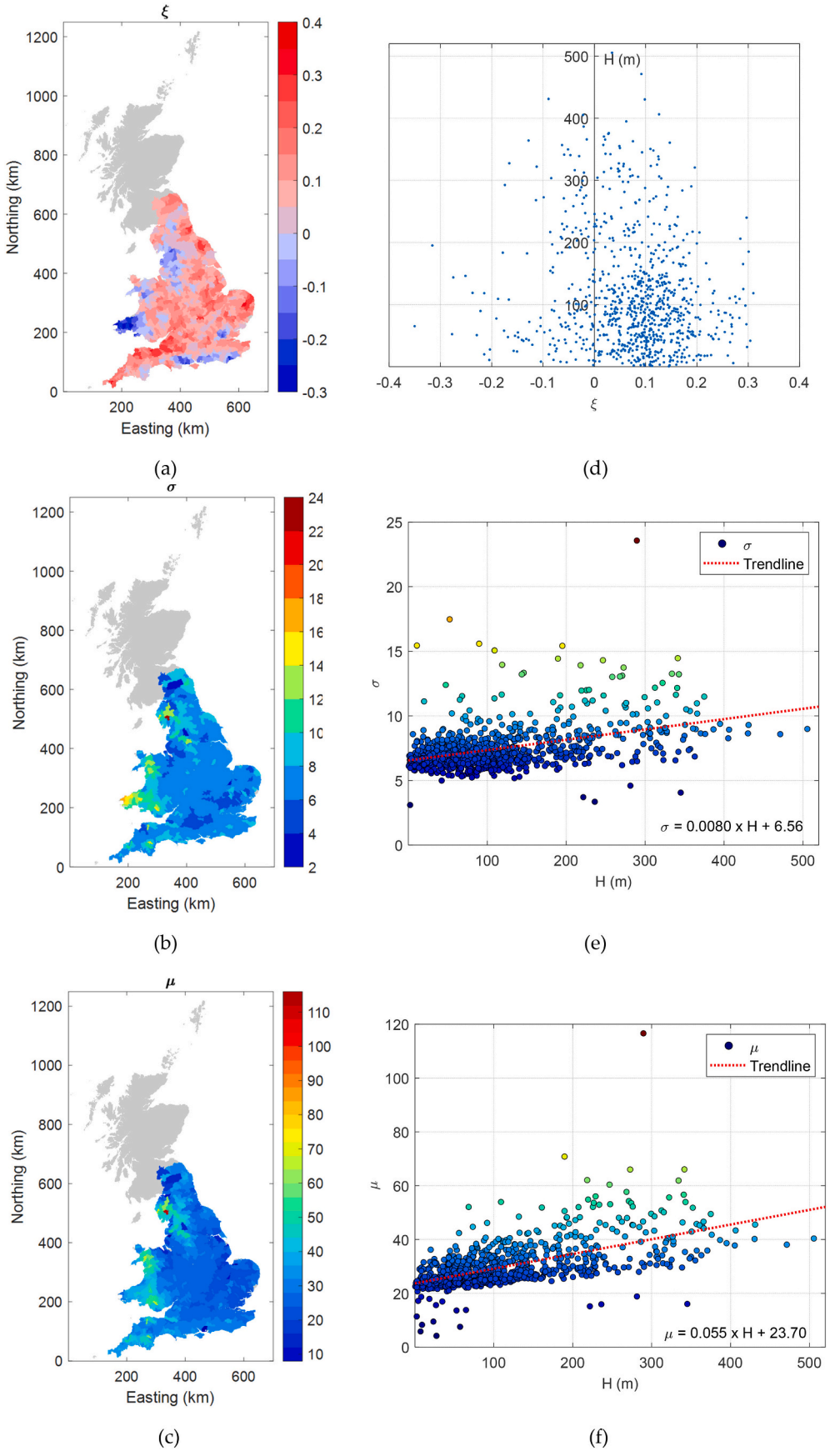

Fig. 5. Spatial variation of AMDR with respect to catchment location represented by the GEV parameters ξ (a), σ (b) and μ (c); and the relationship between these three parameters and the catchment elevation (H) is presented in d,e,f respectively.

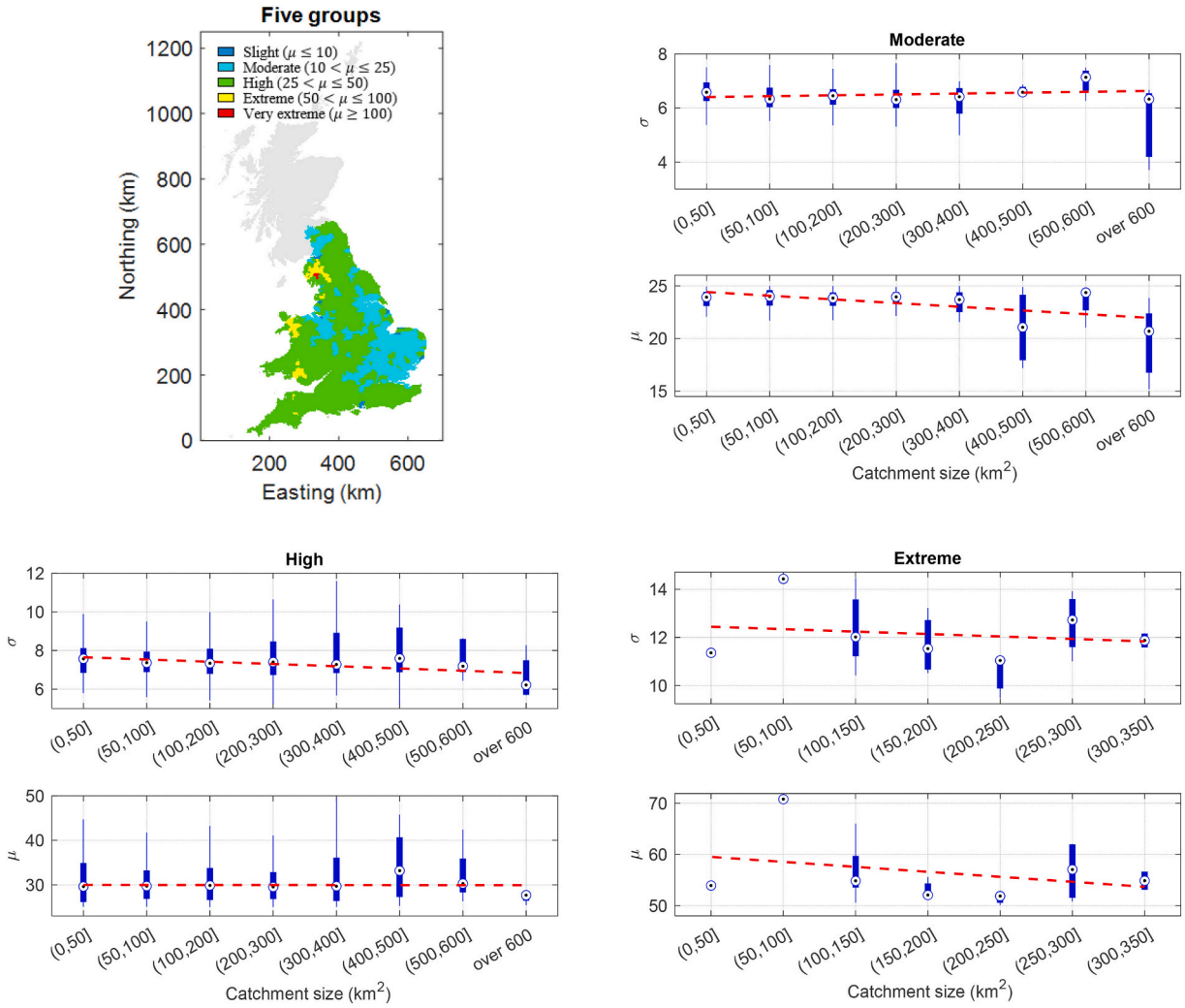

Fig. 6. Categories of the five groups according to the level of AMDR and GEV parameters σ and μ changing with catchment size in the catchments with "Moderate", "High" and "Extreme" levels of AMDR.

inaccurate results. In flood risk management, rainfall is one of the essential inputs of many physically-based models which hydrologists have developed, applied and tested for decades. As the uncertainty, even the error of the model cannot be simply separated from that associated with the rainfall input, understanding the spatial variability and scale in the behaviour of rainfall, especially at extreme levels is important for identifying and analyzing the sensitivity of such spatial variability to the model output. Some publications have assessed the changes of the rainfall input in some catchments e.g., Crespo et al. (2011), Guan et al. (2016), Smith et al. (2004), Shou and Lin (2020), however, they are limited by the number of catchments and not many of them are at the extreme level. More spatial properties should be considered.

In this study, thanks to the developed SPER toolbox, the spatial features such as geographic location, size, orientation and shape can be extracted from an arbitrary catchment and quantified as the specific indexes which are used to further analyse the relationship between these spatial features and hydrological variables. It is specially designed for the new, popular grid-based environmental datasets, which has been ready to apply in many other cases. In our case, we employed the SPER toolbox to extract and quantify the spatial features of more than 900 river catchments in England and Wales and find that most of them (around 99%) are less than 600 km^2 in size while only a few near the boundary between England and Scotland are larger than 1,000 km^2. The catchments in the west tend to be northeast orientated while those near the east coastlines are northwest orientated. The catchments at the boundary between Wales and England tend to be north-south orientated. And the shape of more than half catchments (61%) is relatively rounded or elliptical. Besides, the deviation among the shape of smaller catchments is greater than that of larger catchments and the elongated shape has a much higher probability to be observed in small-sized catchments, however, the large catchment tends to have a relatively rounded shape in England and Wales. These are closely dependent on the topography e.g., the orographic effects of mountains areas in the west where a watershed starts at the highest points on the landscape that divide one valley or drainage from another and lead to the northeast, relatively elongated catchments.

GEV distribution is a widely used distribution for depicting the extreme behaviour of hydrometeorological variables in hydroclimatic science, which can also fit very well in the time series of catchment-based areal annual maximum daily rainfall in England and Wales. The majority of the fitted GEV (around 80%) follow the Fréchet distribution ($\xi > 0$). One of the main results from fitting the GEV model is that those catchments with higher elevation usually get a higher level of the most frequent AMDR and occurrence probability of extremes, as reflected by the GEV parameters μ and σ. The spatial patterns of both μ and σ are similar, which can be described as "west high, east low" with a non-linear change, i.e., there is a significant decreasing trend from west to east, but the gradient of change in the east is much smaller.

Generally, both parameters show a similar decreasing trend when catchment size increases especially in the regions where AMDR is

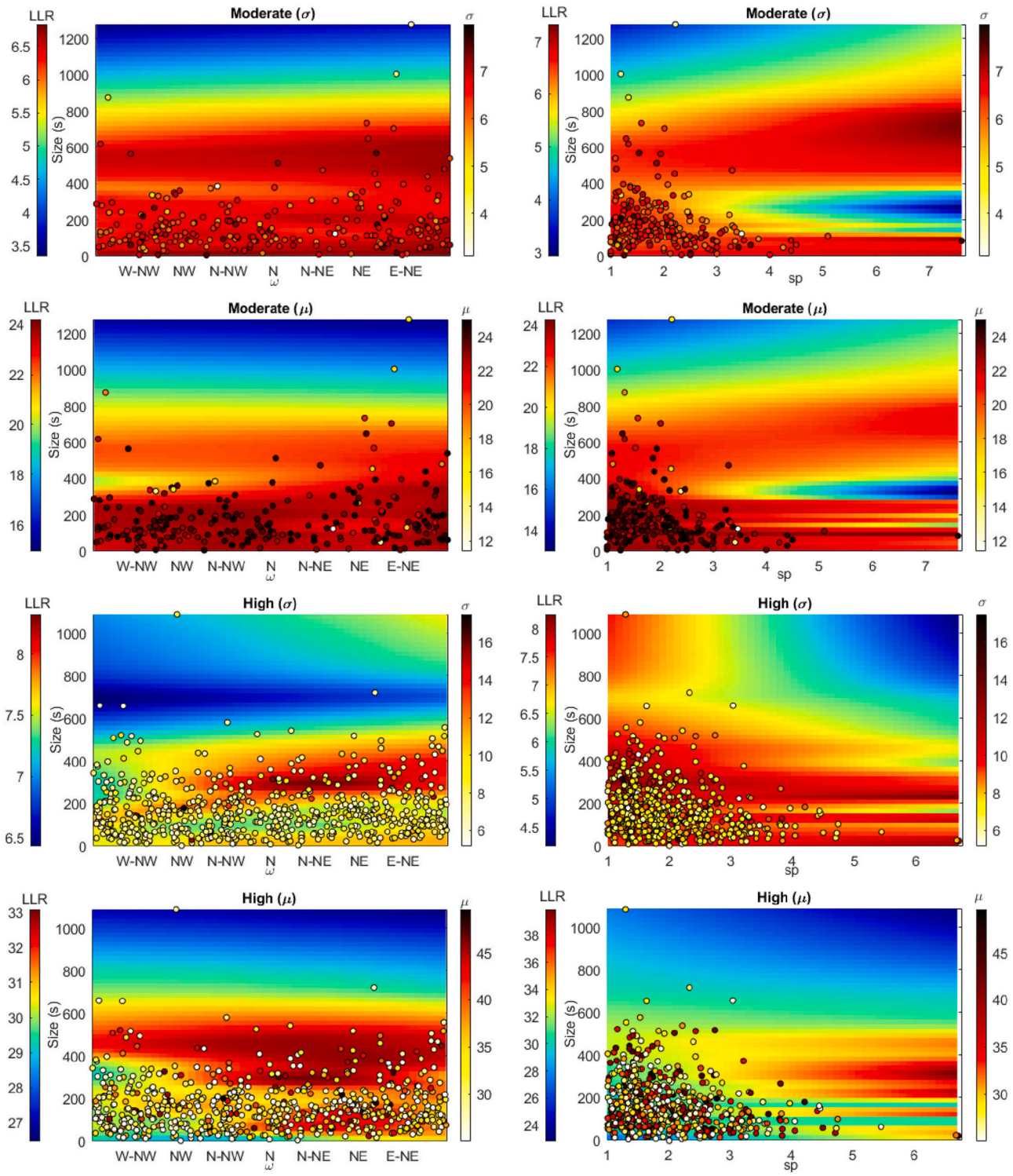

Fig. 7. The GEV parameters σ and μ change over orientation ω (a) and shape *sp* (b) of catchments in the three groups where "LLR" is short for "local linear regression" and the directions "North", "West", "East" are abbreviated as "N", "W" and "E".

relatively moderate or very high. It is because, in these areas such as East England, the Lake District and middle-west Wales, the spatial distribution of grid rainfall is relatively homogeneous thereby such reduction on parameters is mainly caused by statistical average. However, for those catchments having a high level of AMDR especially located at/near the boundary where rainfall changes abruptly, those catchments that have a medium size (e.g., 400– 500 km^2) can witness an increasing trend of parameters with the increase of size. It can be attributed that increasing size in these areas can involve more heterogeneous grid rainfall that the reduction caused by areal average cannot compensate. This phenomenon shows that the change of parameters over catchment sizes can be also affected by their geographic locations.

Compared with other spatial features, the effect of catchment orientation and shape is not as significant, however, several results and

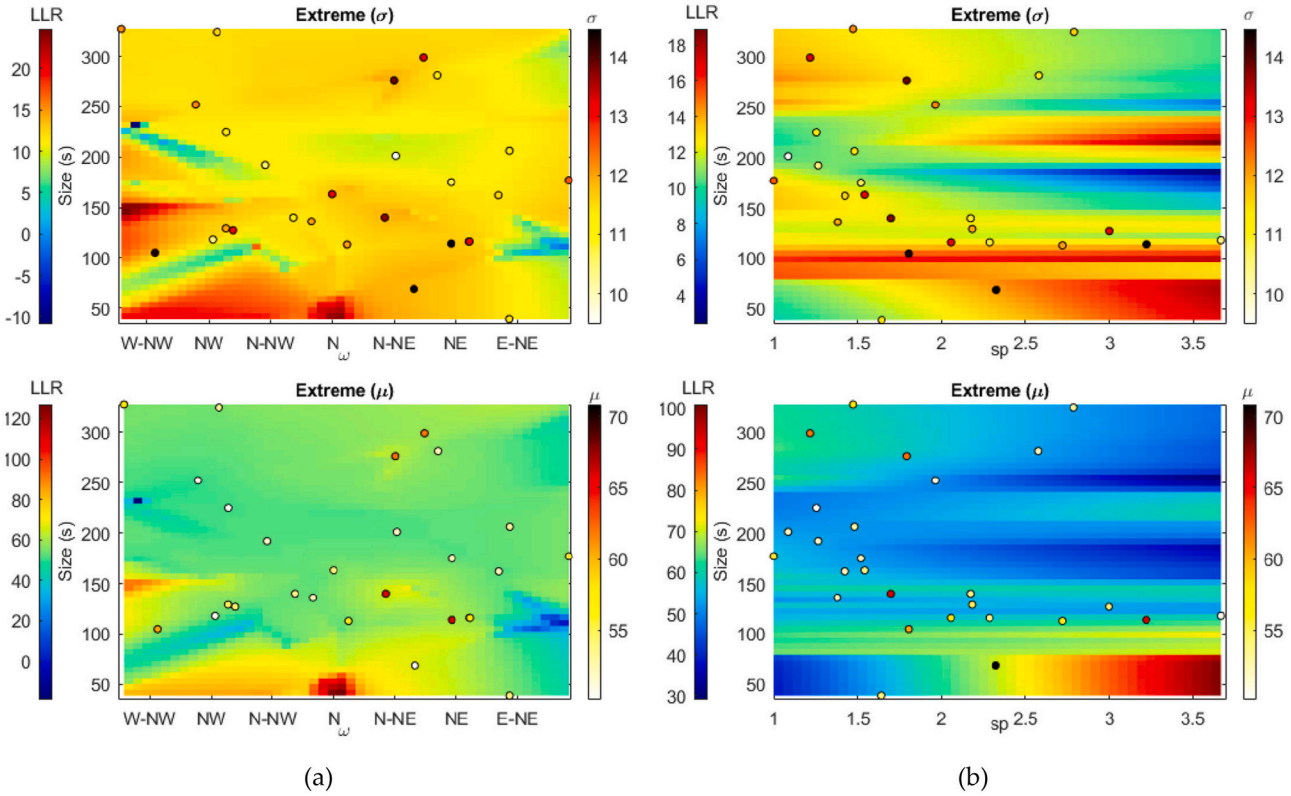

Fig. 7. (*continued*).

the underlying reason are worth studying, which is shown in Fig. 8. The orientations of the relatively-dry catchment with the low level of annual maximum rainfall tend to be east-west dominated ($\omega > 60^o$or $< -60^o$) and the majority are elongated ($sp > 2.5$). However, the catchments that received extreme AMDR have almost different features where the orientation is mainly dominated by north-south (north-northwest or north-northeast; $-45^o \leq \omega \leq 60^o$)) and the shape is relatively rounded ($sp < 1.5$). For the moderate and high level of AMDR, the distribution of orientation is more even when $sp < 3.5$ whilst more catchments are north-west orientated. A possible reason is that the prevailing wind directions in the regional sea of the UK are between south-southwest and northwest (Offshore Energy SEA, *2009*), which brings a huge amount of vapours from the sea and causes extremes rainfall in northwest orientation catchments, especially near coasts.

To be more specific, three widely used statistical tests are employed

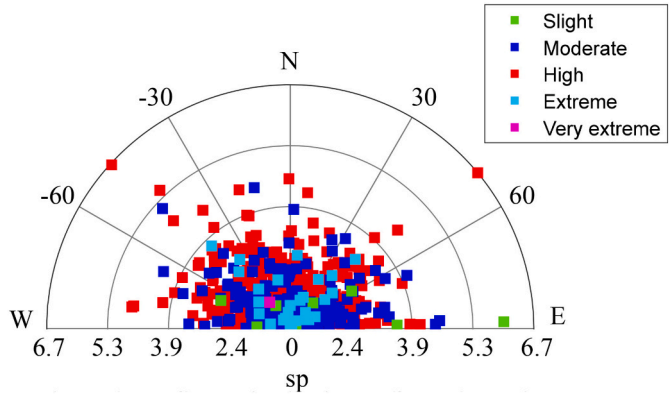

Fig. 8. The distribution of catchments of the five groups with respect to their orientation ω and shape *sp*. The directions "North", "West", "East" are abbreviated as "N", "W" and "E".

to analyse the significance of the impact of these features on the two GEV parameters. The significance level is 0.05 and the features whose *p*-value is less than 0.05 are recognized as significant. More details can be found in supplementary Text S3 while Table 1 presents the correlation coefficient of each feature and the possible combination. Similar to the previous findings, geographic location and elevation are considered as the most significant factors affecting areal rainfall extremes; besides the combined impact of location with size and location with orientation is also significant while the impact of size, orientation and shape are less significant.

However, the correlation among these spatial features and the behaviour of the areal rainfall extremes represented by the GEV parameters does not necessarily imply a causal relationship. This study focuses more on revealing the sampling impacts, i.e., how parameters co-vary with different selections of regions' characteristics. Such 'impacts' from different factors, i.e., the locations, elevation, size, shape and orientation of the catchments, can lead to different determinations of areal rainfall extremes. Surely, the underlying climatology is the driving factor that causes the spatial variation of rainfall extremes, and further work is recommended to explore the link between the climatology and the factors we presented in this study.

5. Conclusions

In this paper, we present a study analyzing the spatial variation of the catchment-oriented extreme daily rainfall of 903 catchments covering England and Wales of Great Britain (GB) by using a century-long grid-based dataset with high spatial and temporal resolutions. Meanwhile, we employed a Spatial Pattern Extraction and Recognition (SPER) toolbox to extract the spatial features of all catchments, i.e., geographic location, elevation, size, orientation and shape. The annual maximum daily rainfall (AMDR) is extracted from each catchment, fitted by Generalized Extreme Value (GEV) distribution and tested by the bootstrapping KS and AD test. The GEV parameters μ and σ are used for

Table 1
The correlation coefficients between catchment features and GEV parameters.

Method	GEV	Catchment Features								
		Location index		Elevation	Size	Orientation	Shape	Combined features		
		x (easting)	y (northing)	H	S	ω	sp	$x \times S$	$x \times sp$	$x \times \omega$
Kendall Test	μ	−0.482*	−0.116*	0.443*	0.017	0.027	0.022	−0.143*	0.029	−0.253*
	σ	−0.255*	0.032	0.288*	0.003	0.012	−0.010	−0.087*	0.011	−0.155*
Spearman Test	μ	−0.668*	−0.162*	0.621*	0.026	0.039	0.033	−0.212*	0.038	−0.371*
	σ	−0.362*	0.0848	0.420*	0.006	0.018	−0.014	−0.131*	0.015	−0.228*
Pearson Test	μ	−0.541*	−0.035*	0.593*	−0.019	0.036	0.022	−0.182*	0.021	−0.282*
	σ	−0.384*	0.086*	0.426*	−0.013	0.026	−0.034	−0.140*	0.021	−0.227*

Note: * indicates that p-value is less than the significance level 0.05.

demonstrating the behaviour of extreme rainfall and quantified with respect to the spatial features of the huge amount of catchments.

These findings highlight that the determination of area rainfall extremes can be affected by the spatial characteristics of the studying catchments and such impacts should be considered for further catchment-based analysis referring to the hydrological response and geomorphic properties. Future work is recommended to investigate closely the underlying datasets with respect to potential inconsistency in the resolution of the data and a comparative study with long-term, single gauge observations are likely to make conclusions more robust.

Data availability

The GEAR dataset and catchments in England and Wales, provided by the Centre of Hydrology and Ecology (CEH), is available in the public domain online at doi:https://doi.org/10.5285/33604ea0-c238-4488-813d-0ad9ab7c51ca for the GEAR dataset and https://nrfa.ceh.ac.uk/content/catchment-boundary-and-areas for more details of catchments; and the elevation of UK (i.e., the OS Terrain 5 dataset) is available at https://www.ordnancesurvey.co.uk/business-government/products/terrain-5. The SPER toolbox employed in the study is available at GitHub (https://github.com/wanghan924/SPER-toolbox). The source code is provided subject to a GPL V3 license.

Declaration of Competing Interest

The authors declare no conflict of interest.

Acknowledgements

The authors would like to thank the UK Centre for Ecology and Hydrology (CEH) for providing the datasets. This research is supported by the Chinese Scholarship Council, China and the College of Engineering, Swansea University, UK via their PhD scholarships offered to the co-author H. Wang, and Academy of Medical Sciences GCRF Networking Grant (REF: GCRFNGR4_1165) for Y. Xuan, which are gratefully acknowledged.

Appendix A. Supplementary data

Supplementary data to this article can be found online at https://doi.org/10.1016/j.atmosres.2021.105968.

References

Anderson, T.W., Darling, D.A., 1952. Asymptotic theory of certain“ goodness of fit” criteria based on stochastic processes. Ann. Math. Stat. 193–212. https://www.jstor.org/stable/2242263.

Anderson, T.W., Darling, D.A., 1954. A test of goodness of fit. J. Am. Stat. Assoc. 49 (268), 765–769. https://doi.org/10.2307/2281537.

Anquetin, S., Braud, I., Vannier, O., Viallet, P., Boudevillain, B., Creutin, J.-D., Manus, C., 2010. Sensitivity of the hydrological response to the variability of rainfall fields and soils for the Gard 2002 flash-flood event. J. Hydrol. 394 (1–2), 134–147. https://doi.org/10.1016/j.jhydrol.2010.07.002.

Archer, D.R., Fowler, H.J., 2018. Characterising flash flood response to intense rainfall and impacts using historical information and gauged data in Britain. J. Flood Risk Manag. 11, S121–S133. https://doi.org/10.1111/jfr3.12187.

Baíllo, A., Grané, A., 2009. Local linear regression for functional predictor and scalar response. J. Multivar. Anal. 100 (1), 102–111. https://doi.org/10.1016/j.jmva.2008.03.008.

Banwell, N., Rutherford, S., Mackey, B., Street, R., Chu, C., 2018. Commonalities between disaster and climate change risks for health: A theoretical framework. Int. J. Environ. Res. Public Health 15 (3), 538. https://doi.org/10.3390/ijerph15030538.

Batisani, N., Yarnal, B., 2010. Rainfall variability and trends in semi-arid Botswana: implications for climate change adaptation policy. Appl. Geogr. 30 (4), 483–489. https://doi.org/10.1016/j.apgeog.2009.10.007.

Buishand, T.A., De Haan, L., Zhou, C., 2008. On spatial extremes: with application to a rainfall problem. Ann. Appl. Stat. 2 (2), 624–642. https://doi.org/10.1214/08-AOAS159.

Burn, D.H., Mansour, R., Zhang, K., Whitfield, P.H., 2011. Trends and variability in extreme rainfall events in British Columbia. Can. Water Resour. J. 36 (1), 67–82. https://doi.org/10.4296/cwrj3601067.

Buytaert, W., Celleri, R., Willems, P., De Bievre, B., Wyseure, G., 2006. Spatial and temporal rainfall variability in mountainous areas: a case study from the south Ecuadorian Andes. J. Hydrol. 329 (3–4), 413–421. https://doi.org/10.1016/j.jhydrol.2006.02.031.

Cleveland, W.S., 1979. Robust locally weighted regression and smoothing scatterplots. J. Am. Stat. Assoc. 74 (368), 829–836. http://www.jstor.org/stable/2286407.

Coles, S.G., Tawn, J.A., 1996. A Bayesian analysis of extreme rainfall data. J. R. Stat. Soc.: Ser. C: Appl. Stat. 45 (4), 463–478. https://doi.org/10.2307/2986068.

Coles, S., Bawa, J., Trenner, L., Dorazio, P., 2001. An Introduction to Statistical Modeling of Extreme Values, Vol. 208. Springer.

Crespo, P.J., Feyen, J., Buytaert, W., Bücker, A., Breuer, L., Frede, H.-G., Ramírez, M., 2011. Identifying controls of the rainfall–runoff response of small catchments in the tropical Andes (Ecuador). J. Hydrol. 407 (1–4), 164–174. https://doi.org/10.1016/j.jhydrol.2011.07.021.

De Haan, L., Ferreira, A., Ferreira, A., 2006. Extreme Value Theory: An Introduction, Vol. 21. Springer.

Eduardo, G., 2020. Notes for Nonparametric Statistics. *Chapter 6 Nonparametric tests* (2021-01-19). https://bookdown.org/egarpor/NP-UC3M/nptests.html (accessed 20 Aug 2021).

Elsebaie, I.H., 2012. Developing rainfall intensity–duration–frequency relationship for two regions in Saudi Arabia. J. King Saud Univ. Eng. Sci. 24 (2), 131–140. https://doi.org/10.1016/j.jksues.2011.06.001.

Embrechts, P., Klüppelberg, C., Mikosch, T., 2013. Modelling Extremal Events: For Insurance and Finance, Vol. 33. Springer Science & Business Media.

Fairman Jr., J.G., Schultz, D.M., Kirshbaum, D.J., Gray, S.L., Barrett, A.I., 2017. Climatology of size, shape, and intensity of precipitation features over Great Britain and Ireland. J. Hydrometeorol. 18 (6), 1595–1615. https://doi.org/10.1175/JHM-D-16-0222.1.

Fan, J., 1993. Local linear regression smoothers and their minimax efficiencies. Ann. Stat. 196-216 https://doi.org/10.1214/aos/1176349022.

Fasano, G., Franceschini, A., 1987. A multidimensional version of the Kolmogorov–Smirnov test. Mon. Not. R. Astron. Soc. 225 (1), 155–170. https://doi.org/10.1093/mnras/225.1.155.

Flanagan, J., Davies, G.H., Boy, F., Doneddu, D., 2020. A review of a distributed high performance computing implementation. J. Inf. Technol. Case Appl. 22 (3), 142–158. https://doi.org/10.1080/15228053.2020.1812803.

Guan, M., Sillanpää, N., Koivusalo, H., 2016. Storm runoff response to rainfall pattern, magnitude and urbanization in a developing urban catchment. Hydrol. Process. 30 (4), 543–557. https://doi.org/10.1002/hyp.10624.

Islam, T., Rico-Ramirez, M.A., Srivastava, P.K., Dai, Q., 2014. Non-parametric rain/no rain screening method for satellite-borne passive microwave radiometers at 19–85 GHz channels with the Random Forests algorithm. Int. J. Remote Sens. 35 (9), 3254–3267. https://doi.org/10.1080/01431161.2014.903444.

Izaguirre, C., Mendez, F.J., Menendez, M., Luceño, A., Losada, I.J., 2010. Extreme wave climate variability in southern Europe using satellite data. J. Geophys. Res. Oceans 115 (C4). https://doi.org/10.1029/2009JC005802.

Jebson, S., 2007. Fact sheet number 3: Water in the atmosphere. http://cedadocs.ceda.ac.uk/id/eprint/255.

Johansson, B., Chen, D., 2003. The influence of wind and topography on precipitation distribution in Sweden: Statistical analysis and modelling. Int. J. Climatol. 23 (12), 1523–1535. https://doi.org/10.1002/joc.951.

Jung, Y., Shin, J.-Y., Ahn, H., Heo, J.-H., 2017. The spatial and temporal structure of extreme rainfall trends in South Korea. Water 9 (10), 809. https://doi.org/10.3390/w9100809.

Kantar, Y.M., Şenoğlu, B., 2008. A comparative study for the location and scale parameters of the Weibull distribution with given shape parameter. Comput. Geosci. 34 (12), 1900–1909. https://doi.org/10.1016/j.cageo.2008.04.004.

Kendon, E.J., Fosser, G., Murphy, J., Chan, S., Clark, R., Harris, G., Lock, A., Lowe, J., Martin, G., Pirret, J., 2019. UKCP Convection-permitting model projections: Science report. https://www.metoffice.gov.uk/pub/data/weather/uk/ukcp18/science-reports/UKCP-Convection-permitting-model-projections-report.pdf.

Kolmogorov, A., 1933. Sulla determinazione empirica di una lgge di distribuzione. *Inst.* Ital. Attuari, Giorn. 4, 83–91.

Kumar, V., Jain, S.K., Singh, Y., 2010. Analysis of long-term rainfall trends in India. Hydrol. Sci. J. 55 (4), 484–496. https://doi.org/10.1080/02626667.2010.481373.

Lilliefors, H.W., 1967. On the Kolmogorov-Smirnov test for normality with mean and variance unknown. J. Am. Stat. Assoc. 62 (318), 399–402. https://doi.org/10.1080/01621459.1967.10482916.

Lobligeois, F., Andréassian, V., Perrin, C., Tabary, P., Loumagne, C., 2014. When does higher spatial resolution rainfall information improve streamflow simulation? An evaluation using 3620 flood events. Hydrol. Earth Syst. Sci. 18, 575–594. https://doi.org/10.5194/hess-18-575-2014.

Lowe, J.A., Bernie, D., Bett, P., Bricheno, L., Brown, S., Calvert, D., Clark, R., Eagle, K., Edwards, T., Fosser, G., 2018. UKCP18 Science Overview Report. Exeter, UK, Met Office Hadley Centre. https://www.metoffice.gov.uk/pub/data/weather/uk/ukcp18/science-reports/UKCP18-Land-report.pdf.

Mann, N.R., 1967. Results on location and scale parameter estimation with application to the extreme-value distribution. In: ROCKETDYNE CANOGA PARK CA. https://apps.dtic.mil/sti/pdfs/AD0653575.pdf.

Moran, G.W., 1984. Locally-Weighted-Regression Scatter-Plot Smoothing (LOWESS): a graphical exploratory data analysis technique. Retrieved from. http://archive.org/details/locallyweightedr1094519419.

Morris, D.G., Flavin, R.W., 1990. A digital terrain model for hydrology. In: Proc 4th Int. Symposium on Spatial Data Handling. Zurich.

Offshore Energy SEA, 2009. Retrieved from. https://assets.publishing.service.gov.uk/government/uploads/system/uploads/attachment_data/file/194346/OES_A3f_Climate_Meteorology.pdf.

Pedersen, L., Jensen, N.E., Christensen, L.E., Madsen, H., 2010. Quantification of the spatial variability of rainfall based on a dense network of rain gauges. Atmos. Res. 95 (4), 441–454. https://doi.org/10.1016/j.atmosres.2009.11.007.

Peleg, N., Marra, F., Fatichi, S., Paschalis, A., Molnar, P., Burlando, P., 2018. Spatial variability of extreme rainfall at radar subpixel scale. J. Hydrol. 556, 922–933. https://doi.org/10.1016/j.jhydrol.2016.05.033.

Phuong, D.N.D., Linh, V.T., Nhat, T.T., Dung, H.M., Loi, N.K., 2019. Spatiotemporal variability of annual and seasonal rainfall time series in Ho Chi Minh city, Vietnam. J. Water Clim. Change 10 (3), 658–670. https://doi.org/10.2166/wcc.2018.115.

Prein, A.F., Liu, C., Ikeda, K., Trier, S.B., Rasmussen, R.M., Holland, G.J., Clark, M.P., 2017. Increased rainfall volume from future convective storms in the US. Nat. Clim. Chang. 7 (12), 880–884.

Sanchez-Moreno, J.F., Mannaerts, C.M., Jetten, V., 2014. Influence of topography on rainfall variability in Santiago Island, Cape Verde. Int. J. Climatol. 34 (4), 1081–1097. https://doi.org/10.1002/joc.3747.

Sangati, M., Borga, M., Rabuffetti, D., Bechini, R., 2009. Influence of rainfall and soil properties spatial aggregation on extreme flash flood response modelling: an evaluation based on the Sesia river basin, North Western Italy. Adv. Water Resour. 32 (7), 1090–1106. https://doi.org/10.1016/j.advwatres.2008.12.007.

Shaw, E., 2005. Hydrology in Practice. CRC Press.

Shou, K.-J., Lin, J.-F., 2020. Evaluation of the extreme rainfall predictions and their impact on landslide susceptibility in a sub-catchment scale. Eng. Geol. 265, 105434 https://doi.org/10.1016/j.enggeo.2019.105434.

Smirnov, N., 1948. Table for estimating the goodness of fit of empirical distributions. Ann. Math. Stat. 19 (2), 279–281. https://doi.org/10.1214/aoms/1177730256.

Smith, M.B., Koren, V.I., Zhang, Z., Reed, S.M., Pan, J.-J., Moreda, F., 2004. Runoff response to spatial variability in precipitation: an analysis of observed data. J. Hydrol. 298 (1–4), 267–286. https://doi.org/10.1016/j.jhydrol.2004.03.039.

Staub, C.G., Stevens, F.R., Waylen, P.R., 2014. The geography of rainfall in Mauritius: modelling the relationship between annual and monthly rainfall and landscape characteristics on a small volcanic island. Appl. Geogr. 54, 222–234. https://doi.org/10.1016/j.apgeog.2014.08.008.

Stott, P.A., Christidis, N., Otto, F.E., Sun, Y., Vanderlinden, J.P., van Oldenborgh, G.J., Vautard, R., von Storch, H., Walton, P., Yiou, P., 2016. Attribution of extreme weather and climate-related events. Wiley Interdiscip. Rev. Clim. Chang. 7 (1), 23–41. https://doi.org/10.1002/wcc.380.

Survey, O., 1946. A Brief Description of the National Grid and Reference System. Retrieved from. https://archive.org/details/NationalGridDescriptionOrdnanceSurvey1946HMSOImages/page/n3/mode/2up.

Tanguy, M., Dixon, H., Prosdocimi, I., Morris, D.G., Keller, V.D.J., 2016. Gridded Estimates of Daily and Monthly Areal Rainfall for the United Kingdom (1890-2015) [CEH-GEAR]. NERC Environmental Information Data Centre. https://doi.org/10.5285/33604ea0-c238-4488-813d-0ad9ab7c51ca.

Taylor, C.M., Belušić, D., Guichard, F., Parker, D.J., Vischel, T., Bock, O., Harris, P.P., Janicot, S., Klein, C., Panthou, G., 2017. Frequency of extreme Sahelian storms tripled since 1982 in satellite observations. Nature 544 (7651), 475–478. https://doi.org/10.1038/nature22069.

Tomasella, J., Sene Gonçalves, A., Schneider Falck, A., Oliveira Caram, R., Rodrigues Diniz, F., Rodriguez, D., Rodrigues do Prado, M., Negrão, A., Sueiro Medeiros, G., Chagas Siquiera, G., 2019. Probabilistic flood forecasting in the Doce Basin in Brazil: Effects of the basin scale and orientation and the spatial distribution of rainfall. J. Flood Risk Manag. 12 (1), e12452 https://doi.org/10.1111/jfr3.12452.

Villarini, G., Smith, J.A., Baeck, M.L., Sturdevant-Rees, P., Krajewski, W.F., 2010. Radar analyses of extreme rainfall and flooding in urban drainage basins. J. Hydrol. 381 (3–4), 266–286. https://doi.org/10.1016/j.jhydrol.2009.11.048.

Wang, H., Xuan, Y., 2020. Spatial variation of extreme rainfall observed from two century-long datasets. Geophys. Res. Lett https://doi.org/10.1029/2020GL091933 e2020GL091933.

Zheng, Y., Xue, M., Li, B., Chen, J., Tao, Z., 2016. Spatial characteristics of extreme rainfall over China with hourly through 24-hour accumulation periods based on national-level hourly rain gauge data. Adv. Atmos. Sci. 33 (11), 1218–1232. https://doi.org/10.1007/s00376-016-6128-5.